Journal of Techniques, ISSN: 2708-8383, Vol. 7, No. 1, 2025, Pages 66-79
DOI: https://doi.org/10.51173/jt.v7i1.2625

JOURNAL OF TECHNIQUES

Journal homepage: http://journal.mtu.edu.iq

RESEARCH ARTICLE - ENGINEERING (MISCELLANEOUS)

Investigating the Changes of Dissolved Substances in Water Using Remote Sensing (Case Study: Al-Gharraf River)

Salwa Mohammed Hasan Abbas[1*], Amir Shahrokh Amini[1]

[1]Department of Surveying - Remote Sensing, College of Engineering, Islamic Azad University, Tehran, Iran

[*] Corresponding author E-mail: salwaalmayah@gmail.com

Article Info.

Article history:

Received
24 September 2024

Accepted
03 February 2025

Publishing
31 March 2025

Abstract

Water quality monitoring is important for water resource management, but traditional methods are expensive and limited. Remote sensing provides a practical solution to access accurate information at the lowest cost and in the fastest time. The research aims to study the changes in dissolved materials in the water of the Al-Gharraf River, which is located in the Al-Hay area in Wasit Governorate and is considered one of the main sources of surface water in Iraq. Seasonal data (winter and summer of 2021 and 2022) of water quality parameters collected from the water quality monitoring station in the study area were taken as field observations, and Landsat 8 images formed the remote sensing data for the research. Landsat images were processed using the maximum likelihood classification (MLC) algorithm and water bodies in the area were identified. The performance of MLC was evaluated with precision and precision criteria. The average classification accuracy for the train data was 0.954 and 0.970, and for the test data, they were 0.936 and 0.97, respectively. To detect water bodies, the correlation between six spectral bands, two spectral indices, and 12 different combinations of spectral bands and water quality parameters was calculated using Pearson's coefficient. The results were different depending on the qualitative criteria, but the observed high correlation coefficients showed that the remote sensing data used in the research were useful for monitoring changes in dissolved materials in the water of the Garraf River. The spatial trend of changes was analyzed by the Mann-Kendall test and the temporal trend was analyzed by fifth-order polynomial fitting. The study revealed uniform spatial and seasonal changes in river water quality standards, which affect the environment, aquatic life, and citizens. Landsat satellite data provide valuable information to monitor these changes and help decision makers manage water resources effectively.

Publisher: Middle Technical University

Keywords: Remote Sensing; Water Quality Monitoring; Al-Gharraf River; Satellite Image Classification; Water Dissolved Substances Changes.

1. Introduction

Water is a valuable natural resource essential for human survival and ecosystem health. Nearly half of the world's population lives on the shores of seas, lakes and rivers, and their number is constantly increasing. Riverbanks and other aquatic areas are very sensitive environments with fragile ecosystems, and any changes caused by human activities in them could endanger the habitat of fish and other aquatic organisms [1]. In addition, access to sustainable urban water sources requires continuous monitoring of the quality of existing water sources and their watersheds. Knowing the level of water purification required for human use, agriculture, animal husbandry, and industry also requires an understanding of water quality resources. Therefore, the importance of water quality monitoring should be considered more than ever, and the concentration of chemicals in wastewater and industrial discharges into water should be strictly controlled. [2, 3]. Traditionally, water quality indicators (physical, chemical and biological properties) are determined by collecting samples from water sources and then examining them in a laboratory. This method is very accurate, but it is a time-consuming and heavy process. Therefore, establishing a timely database of water quality at the regional level is not possible [4]. Another limitation of this method is the lack of identification of spatial and temporal changes in water quality, which is vital for comprehensive management of water resources. Therefore, the difficulties and limitations of traditional methods have become an important obstacle to water quality monitoring and management. This research aims to study the changes in dissolved materials in the water of the Al-Gharraf River, one of the main sources of surface water in Iraq, flowing through the Al-Hay District in Wasit Governorate. The research also aims to provide a solid basis for tracking changes in the dissolved compounds in the river's water through Landsat satellite data. This approach can provide decision-makers with useful information to manage water resources as effectively as possible.

1.1. Problem statement

The Gharraf River branches off from the Tigris River near the city of Kut and flows through the Wasit and Dhi Qar governorates in southern Iraq. It is the main water source for agriculture and public water supply and has impacts on the social and economic aspects of the region [5].

The river receives most of the wastewater resulting from many activities, such as water passing through agricultural and domestic areas and some sewage and industrial wastewater. In general, humans can be considered the main cause of water pollution and the decline in its quality.

Nomenclature & Symbols			
GIS	Geographical Information System	USGS	United States Geological Survey
MSI	Multispectral Instrument	CEOS	Committee on Earth Observation Satellites
TDS	Total Dissolved Solids	OLCI	Ocean and Land Color Instrument
EC	Electrical Conductivity	MCI	Maximum Chlorophyll Index
Turb	Turbidity	GNDVI	Green Normalized Difference Vegetation Index
NDTI	Normalized Difference Turbidity Index	NDBI	Normalized Difference Built-up Index
NDVI	Normalized Difference Vegetation Index	NDWI	Normalized Difference Water Index
BSI	Bare Soil Index	SWIR	Short-Wave Infrared
NIR	Near Infrared		

The development of the region and the decrease in water levels in the river have also led to an increase in pollutants, which is a cause for concern [6].

The concentration of salts in sea and river water is affected by several factors, the most important of which are: evaporation rates, average temperature, solar radiation, and air humidity. There is no doubt that evaporation rates and rates of rain or snowfall will affect the salinity of seas and rivers, which vary depending on the location of the latitude circle and the season of the year. The negative consequences of water pollution on human health and the environment are visible. Statistics indicate the impact on people's health due to the consumption of poor-quality water. Today, easy access to free remote sensing data has created a well-suited capacity for water quality monitoring in less developed regions [7]. In addition, remote sensing offers the possibility of retrieving current and past information from water sources that were not part of the ground-based sampling program [8]. However, limited studies have used remote sensing capabilities to monitor the quality of water resources in Iraq. Therefore, further study is needed in this area and the results of the current study can also help in the management of water resources in this country.

1.2. Importance of the study

The water quality of Iraq's rivers is no longer safe enough for consumption [9]. This problem made Iraq face a serious threat. The Gharraf River is the main branch of the Tigris River in southern Iraq, which suffers from natural and human problems such as pollution, mud accumulation, plant growth such as water hyacinth, waste, and low water levels. This river provides water for the lives of millions of people who live near its basin and runs through a very large agricultural area within the alluvial plain. In addition, the high fluctuations in the annual discharge of this river increase the turbidity and dissolved matter in its waters [10]. The negative effects of water pollution on human health and the environment are evident. Statistics show that thousands of people die every day due to the consumption of poor-quality water, and people who live in less developed regions such as Iraq are more at risk [11]. Today, easy access to free remote sensing data has created a very suitable capacity for monitoring water quality in less developed regions [12]. In addition, remote sensing offers the possibility of retrieving current and past information from water sources that were not part of terrestrial sampling programs [13]. However, limited studies have used remote sensing capabilities to monitor the quality of water resources in Iraq. Therefore, it is felt that more study is needed in this field and the results of the current study can also help in the management of water resources in this country.

1.3. Objectives

Studies indicate that the water quality of the Gharraf River fluctuates over time. In addition, the length of this river and its passage through many urban and agricultural areas led to the possibility of the presence of many sources of pollution in its various sections. Remote sensing enables spatial and temporal environmental monitoring. Therefore, the primary objective of this study is to study the variations of dissolved substances in Gharraf water through remote sensing. To identify the various sources of pollution in the Gharraf River, these changes will be studied spatially and seasonally over time.

2. Foundations and Literature Review

2.1. Water quality monitoring with remote sensing

Monitoring water quality is an essential aspect of water resources management. Examining water quality with conventional methods is a time-consuming and expensive endeavor that yields point-by-point data. This information is only applicable to the measurement location and has location- and time-specific limitations. Consequently, the combination of remote detection and on-site measurements is extremely beneficial. The spectral behavior of water varies depending on its quality. Therefore, the existence of a meaningful relationship between in situ water quality parameters and spectral values of image pixels is the basis of remote sensing water quality monitoring. Water quality can be obtained by using specific parts of the electromagnetic spectrum, such as the visible and infrared regions, where the water absorbs the majority of the radiation that reaches it, and only a small amount of its value is reflected in the sensor. The amount of this reflection will decrease as the wavelength increases [14]. In remote sensing images, unadulterated water has the darkest color and behaves like an ebony body. When the impurities and contaminants of water increase, the sensor receives greater reflection, and the turbidity of the imaged water decreases.

2.2. Spectral indices of satellite images

The spectral indices of satellite images are straightforward mathematical relationships between multiple spectral indices that provide new information. There are a variety of mathematical operators that can be used to generate spectral indices, but division, subtraction, addition, and multiplication are the most common. There are numerous applications for spectral indices in various disciplines, such as identifying features, minimizing the effect of shadows and topography, enhancing the classification and modeling of satellite images, and monitoring changes in phenomena [15]. Among the most common spectral indices are the Normalized Difference Built-up Index (NDBI) and the Normalized Difference Vegetation Index (NDVI), the Normalized Difference Water Index (NDWI), and the Bare Soil Index (BSI):

- NDBI is one of the spectral indices used to identify artificial surfaces. This index identifies artificial surfaces using short-wave infrared (SWIR) and near-infrared (NIR) bands [16]:

$$NDBI = (SWIR - NIR) / (SWIR + NIR) \quad (1)$$

- NDVI is a dimensionless index that considers the normalized difference between visible red and NIR reflectance to describe vegetation cover. This index can estimate the density of green color in an area [17]:

$$NDVI = (NIR - Red) / (NIR + Red) \quad (2)$$

- NDWI is used to identify and monitor changes in water bodies. Water bodies strongly absorb light in the visible to the infrared electromagnetic spectral bands. Therefore, NDWI uses green and NIR bands to detect water bodies [18]:

$$NDWI = (Green - NIR) / (Green + NIR) \quad (3)$$

- BSI uses a combination of Blue, red, NIR, and SWIR spectral bands to determine soil changes. The SWIR and red bands are used to determine the mineral composition of the soil, and the NIR and blue bands are used to determine the vegetation cover [19].

$$BSI = ((Red + SWIR) - (NIR + Blue)) / ((Red + SWIR) + (NIR + Blue)) \quad (4)$$

In addition to the introduced spectral indices, researchers have shown that the Red, Green, and Blue spectral bands of Landsat images and their combinations are useful for monitoring salinity and dissolved substances in water sources. [20]:

$$\text{Index 1} = \sqrt{\text{Red} \times \text{Green}} \quad (5)$$

$$\text{Index 2} = \sqrt{\text{Blue} \times \text{Green}} \quad (6)$$

$$\text{Index 3} = \text{Blue} \times \text{Green} \quad (7)$$

$$\text{Index 4} = \text{Blue} \times \text{Red} \quad (8)$$

$$\text{Index 5} = \text{Blue} \times \text{Green} \times \text{Red} \quad (9)$$

2.3. Maximum likelihood classification (MLC) algorithm

MLC is one of the most popular image classification methods in remote sensing. In this supervised algorithm, each pixel is classified in its corresponding class with the highest probability. MLC is based on Bayes theorem and defines the probability that a pixel with feature vector w belongs to class i as follows [21].

$$P(i|w) = \frac{P(w|i)P(i)}{P(w)} \quad (10)$$

In Eq. 10, P(w|i) is the likelihood function, P(i) is the probability of occurrence of class i in the study area (prior information) and P(w) is the probability of observing w, which is determined as follows:

$$P(w) = \sum_{i=1}^{M} P(w|i)P(i) \quad (11)$$

In Eq. 11, M is the number of classification classes. Often P(w) is taken as a normalization constant to ensure Eq.11 is correct. Pixel x is assigned to class i by Eq. 12:

$$\sum_{i=1}^{M} P(w|i) = 1 \quad (12)$$

$$x \in i \quad \text{if} \quad P(i|w) > P(j|w) \quad \text{for all } j \neq I \quad (13)$$

In Eq. 13, each pixel is assigned to the class with the highest probability or is assigned as an unclassified sample if its probability values in all classes are below a user-defined threshold [22].

2.4. Classification of satellite images

Satellite photos are employed in a variety of issues related to meteorology, agriculture, geology, urban planning, natural sciences, earth sciences, and creating land cover maps because satellites give images with varying geographical and temporal resolutions all over the world [23]. These photos include a variety of spectrum data. This information can be categorized according to its intended use, which gives the necessary data for study. The pixel-based method and the object-oriented method are typically used to categorize satellite photos. The pixel-based method has been the main approach for classifying satellite images for many years. In this method, using an algorithm, pixels are placed in similar classes based on their spectral values [24]. In the object-oriented method, the pixels are divided into homogeneous and heterogeneous groups before classification based on their spectral values and form image objects. Then, like the pixel-based method, image objects are placed in similar classes using an algorithm [25]. Recently, the use of the object-oriented method has become very common. Many studies have stated that the performance of this method is better than the pixel-based method. However, in some research, there is not much difference between these two methods [26].

3. Methodology

This study was conducted in two main steps to classify land cover and investigate changes in dissolved matter in water. Accordingly, in the first step, Landsat 8 images were collected, and various spectral bands and indices were extracted from them. Then, 2000 random sample points were selected in the study area and their land cover class was determined by visual inspection. The outputs of the mentioned steps formed a land cover classification dataset using confusion matrix, accuracy and precision criterion. 500 random points were selected and distributed over the study area for land cover classification and the MLC algorithm was trained using 75% of this dataset and validated using the remaining 25%. Then, water bodies were distinguished from other land cover classes. In the second step, using Landsat 8 images again, various spectral bands and indices were extracted for the water bodies identified in the previous step. Then, the correlation between the values of these extracted

variables and the values obtained from in situ measurements of dissolved matter in water was analyzed. After analyzing the correlation using Pearson's correlation coefficient to determine the low, medium and high correlation values and by examining the spectral ranges and indicators that were highly correlated with the number of dissolved materials in the water, the spatial and seasonal changes of dissolved materials in the water of the Garraf River were evaluated as shown in Fig.1.

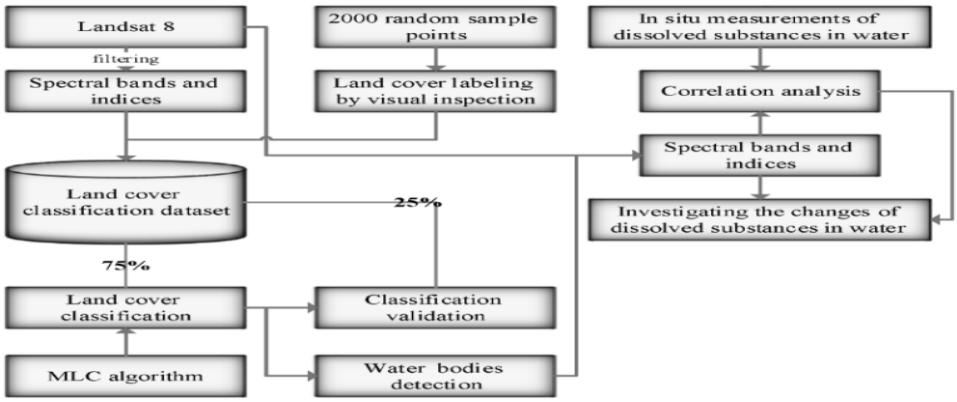

Fig. 1. Methodology

3.1. Study area

The Al-Gharraf River flows from the Al-Kut Dam on the right bank of the Tigris into the Euphrates basin, through the governorates of Wassit and Dhi Qar, and into the Al-Hammar Marsh to the north of Nassyria City. The principal tributary of the Tigris River has a maximal capacity of 622 cubic meters per second, an approximate length of 230 kilometers, and a discharge area of 435,052 x 10^6 square meters. The Al-Gharraf River utilizes 52 canals and 968 channels to irrigate a 700,000-hectare area. Al-Gharraf River is located between 48°45' and 46°17' east longitude and 31°4' and 32°30' north latitude, where the climate is semi-arid (high temperature in summer, low moisture, little annual rainfall, high solar radiation rate, and high evaporation rate [26]. Fig. 2 depicts the research area as a portion of the Al-Gharraf River in the Al-Hai region of the Wasit governorate.

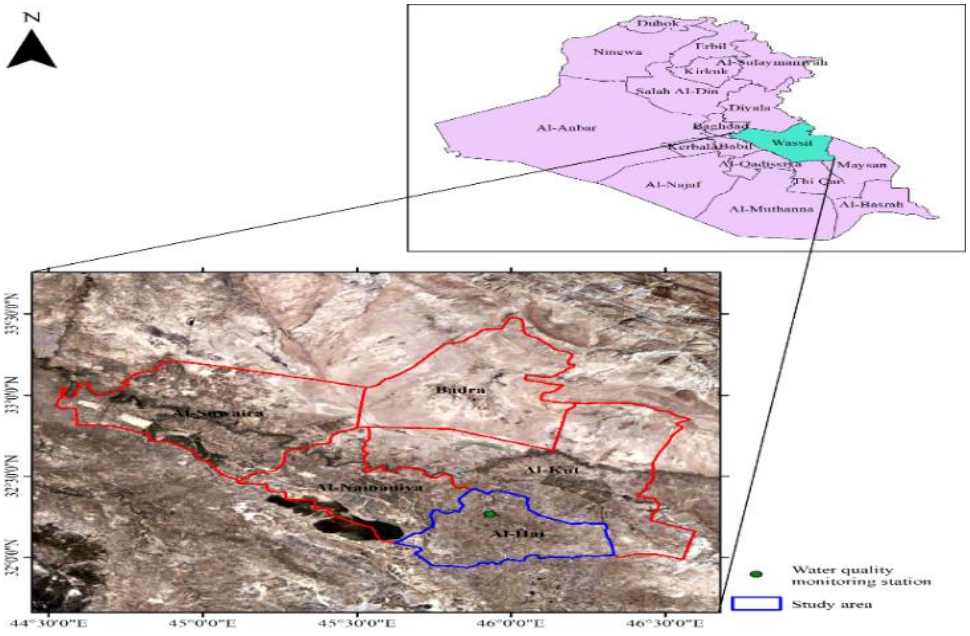

Fig. 2. Study area

3.2. Dataset

3.2.1. Satellite images dataset

In this investigation, the United States Geological Survey (USGS) dataset Landsat 8 - Collection 2 - Level 2 was used. This dataset was released at the beginning of 2021 with enhanced geometric precision, processing, and radiometric calibration in comparison to earlier products. In addition, the Committee on Earth Observation Satellites (CEOS) has confirmed that the Landsat 8 - Collection 2 - Level 2 dataset permits users to conduct swift analyses with minimal processing requirements (Digital-Earth-Africa, 2021) [27]. The cited dataset contains surface reflectance and surface temperature data, of which the surface reflectance data was utilized in the current study. Surface reflectance is the fraction of solar radiation reflected from the earth's surface. Changes in satellite-measured radiation caused by atmospheric characteristics have been corrected, making it possible to compare images obtained from the same area at different times (Digital-Earth-Africa, 2021).

3.2.2. Water quality dataset

The data on water quality was collected at the monitoring station in the Wassit governorate. This station's location is displayed in Fig.3. This dataset contains the January and July 2021 and 2022 values for phosphate (PO4), nitrate (NO3), calcium (Ca), magnesium (Mg), potassium (K), sodium (Na), sulfate (SO4), chlorine (CL), total dissolved solids (TDS), electrical conductivity (EC), and turbidity (Turb). Table 1 is a breakdown of the water quality data set (Water quality data were collected from Wasit Water Station located in Al Kut Governorate).

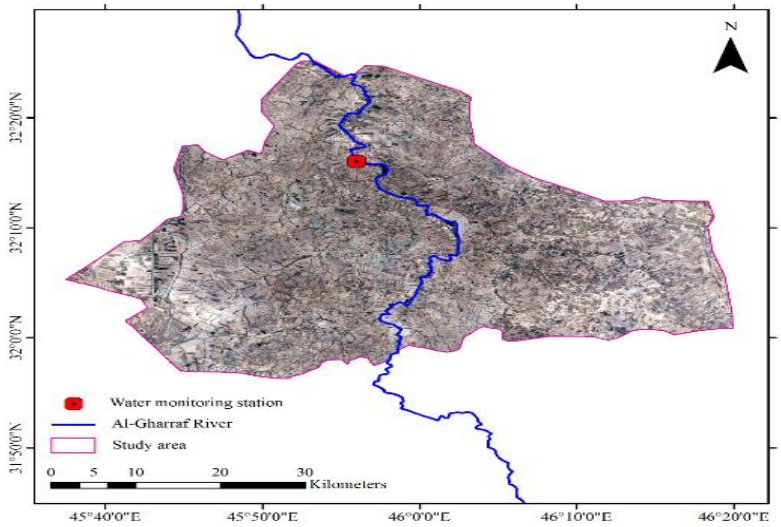

Fig. 3. Location map of the water monitoring station

Table 1. Details of the water quality dataset

Parameter	Value (January 2021)	Value (July 2021)	Value (January 2022)	Value (July 2022)
PO4	0.28	0.28	0.22	0.32
NO3	4.7	4.8	5.8	5.4
Ca	124.2	80	88.4	69.2
Mg	32.4	34	24.2	25.4
K	4.8	5.2	5.8	5.8
Na	100.5	110	105	120
SO4	325	326	269	276
Cl	127.4	125.4	129.3	141.12
TDS	844	820	848	770
EC	1294	1186	1236	1120
Turb	49.7	15.6	19.6	54.4

-Water quality data were collected from Wasit Water Station located in Al Kut Governorate**.**

3.2.3. Land cover classification

MLC algorithm was used in ArcGIS 10.5 software to classify land cover and determine water resources. This classifier is available from Toolboxes\System Toolboxes\Spatial Analyst Tools. tbx\Multivariate\Maximum Likelihood Classification in ArcGIS 10.5. The classifier parameter was considered as default, and its tuning and optimization were omitted. Accordingly, the value of the rejection fraction parameter was equal to zero and the value of the a priori_probabilities parameter was EQUAL.

The rejection fraction parameter specifies the probability threshold of assigning a cell to a class. This means that if the probability of assigning the cell to all classes was lower than the threshold value, the cell would not be classified. The zero value of this parameter means that all cells were classified. The parameter a_priori_probabilities specifies how to determine the prior probabilities (prior information). The value of this parameter was EQUAL. Therefore, all classes had the same prior probability.

3.2.4. Classification validation parameters

The confusion matrix is one of the performance measurements for classification algorithms in two or more class problems. The confusion matrix is a Table 1 containing four distinct combinations of predicted and observed values. Four true positive (TP) and true negative (TN) variables, false positive (FP) and false negative (FN) make up the values of Table 1:

- TP is the number of positive samples that are predicted positive.
- TN is the number of negative samples that are predicted negative.
- FP is the number of negative samples that are predicted to be positive.
- FN is the number of positive samples that are predicted negative.

Using the aforementioned definitions, the parameters of precision and accuracy can be determined. Accuracy is the ratio of correct predictions to the total number of predictions, and the ratio of correct positive predictions to the total number of positive predictions. The higher the value of these two parameters, the better the performance of the classifier.

$$Accuracy = \frac{TP+TN}{TP+TN+FP+FN} \quad (16)$$

$$Precision = \frac{TP}{TP+FP} \quad (17)$$

3.2.5. Monitoring water dissolved substances

To monitor dissolved substances in river water, the correlation between the values of the dissolved substances and the spectral band and spectral index values of Landsat images must be calculated. By calculating the correlation, dissolved substances in water at locations other than the water quality monitoring station can be estimated using satellite images. Pearson's correlation coefficient is used to determine the correlation between two variables. This coefficient is calculated by dividing the covariance of two variables by multiplying their standard deviation (Eq. 18).

$$\rho \, x, y = corr\,(x,y) = \frac{cov(x,y)}{\sigma_x \sigma_y} = \frac{E[(x-\mu_x)(y-\mu_y)}{\sigma_x \sigma_y} \quad (18)$$

In Eq.18, ρ is the population correlation coefficient, x and y are random variables, μx and μy are expected values, σx and σy are standard deviation values, E is the expected value operator, and cov is the covariance value.

3.2.6. Trend analysis with Mann-Kendall test

The Mann-Kendall test can be used to analyze the trend of a variable. This test was first created by Mann in 1945, then Kendall developed it in 1966. This statistical test is based on the comparison of the H0 and H1 hypotheses and decides by rejecting or accepting the H0 hypothesis. H0 indicates that the variable is random and there is no trend in the data series and rejecting the H0 (accepting the H1) means there is a trend in the data series. The calculation of the Mann-Kendall statistic begins by calculating the difference between data records and then applying the sgn function (Eq.19) [28].

$$S = \sum_{k=1}^{n-1} \sum_{j=k+1}^{n} sgn(x_j - x_k) \quad (19)$$

$$sgn(s) = \begin{cases} +1 \;\; if \; (x_j - x_k) > 0 \\ -1 \; if \; (x_j - x_k) = 0 \\ 0 \;\; if \; (x_j - x_k) < 0 \end{cases} \quad (20)$$

According to Eq.20, sgn function outputs are 0, +1, and -1. The variance of S is obtained by Eq.21.

$$\text{var (s)} = \frac{n(n-1)(2n+5) - \sum_{i=1}^{m} t_i(t_i-1)(2t_i+5)}{18} \quad (21)$$

In Eq.18, n is the number of data records, m is the number of tied groups, and t_i Equals the number of data records in the p th group. Finally, the Z_{MK} statistic is calculated by Eq.22.

$$Z_{MK} = \begin{cases} \frac{S-1}{\sqrt{var(s)}} \; if \; S > 0 \\ 0 \; if \; S = 0 \\ \frac{S+1}{\sqrt{var(s)}} \; if \; S < 0 \end{cases} \quad (22)$$

If Z_{MK} is positive, th upward trend is considered, and if it is negative, the downward trend of the data series is considered. H0 (no monotonic trend) is rejected and H1 (upward monotonic trend) is accepted if:

$$Z_{MK} \geq Z_{1-\alpha} \quad (23)$$

H0 (no monotonic trend) is rejected and H1 (downward monotonic trend) is accepted if:

$$Z_{MK} \leq -Z_{1-\alpha} \quad (24)$$

H0 (no monotonic trend) is rejected and H1 (upward or downward monotonic trend) is accepted if:

$$|Z_{MK}| \leq \frac{Z_{1-\alpha}}{2} \quad (25)$$

α is the tolerable probability that the Mann-Kendall test will falsely reject the H0.

3.2.7. Trend analysis by graphing

Another trend analysis method is graphing. Different graphs can be used to understand the trend of the data series . However, linear regression is one of the best methods for graphing and trend analysis. The interaction of time and variable values determines the graph points and regression tries to find a function that passes through all these points with the least error. An n-the polynomial is defined as a regression function by Eq. 26. In Eq.25, x is the independent variable (time), y is the dependent variable (variable value), and n is the constant coefficient.

$$y = \sum_{i=0}^{n} a_n \times x^n \quad (26)$$

A polynomial is fitted by reaching the optimal values of a. The least squares method can reach the values. This method can solve systems of equations where the number of observations is more than the number of variables. In the least square method to fit the function y = f(x, a) to sample points, the residual is defined as follows:

$$d_i = y_i - f(x_i, a_i) \quad (27)$$

If y_i follows a normal distribution around $f(x_i, a_i)$ values with the threshold of $\sigma_{y,i}$, the probability of observing all y values is as follows:

$$Prob_a(y_1, y_2, \dots, y_n) = Prob_{a_1}(y_1) \times Prob_{a_2}(y_2) \times \dots \times Prob_{a_n}(y_n) \propto \frac{e^{-x^2/2}}{\prod_{i=1}^{n} \sigma_{y,i}} \quad (28)$$

The x^2 parameter is calculated by Eq. 29.

$$x^2 = \sum_{i=1}^{n} \frac{(y_i - f(x_i, a_i))^2}{{\sigma_{y,i}}^2} = \sum_{i=1}^{n} \frac{{d_i}^2}{{\sigma_{y,i}}^2} \quad (29)$$

By finding the values in such a way that x^2 is minimized, the least squares problem is solved. Accordingly, we have:

$$\frac{\partial x^2}{\partial a_i} = 0, i = 1, \dots, n \quad (30)$$

4. Results

4.1. Introduction

Using Landsat images and the MLC model with its default parameters, a land cover map of the study area and an estimate of the Al-Gharraf River's boundary were generated. The inputs of the MLC model are summarized in Table 2. After constructing the land cover map, the correlation between spectral bands and indices and water quality parameters measured at the water quality monitoring station was computed in Table 1. These calculated correlation values can be used to estimate water quality in areas where in situ measurements are unavailable. Table 3 displays the spectral bands and indices used to compute correlation values.

Table 2. Modeling inputs for the MLC algorithm

Independent variable		Dependent variable
Spectral band	Spectral indices	Land cover class
Red	BSI	Water class
Green	NDBI	Non-water class
Blue	NDVI	
SWIR 1	NDWI	
SWIR 2		
NIR		

Table 3. Spectral bands and indices used for calculating the correlation of water quality parameters

Spectral band	Spectral indices		
Red	NDVI	$\sqrt{\text{Red} \times \text{Blue}}$	$\sqrt{\text{SWIR1} \times \text{Green}}$
Green	NDWI	$\sqrt{\text{Red} \times \text{Blue} \times \text{Green}}$	$\sqrt{\text{SWIR 2} \times \text{Green}}$
Blue	Red X Green	NIR × Green	
NIR	Red x Blue	SWIR1 × Green	
SWIR 1	Red x Blue x Green	SWIR 2 × Green	
SWIR 2	$\sqrt{\text{Red} \times \text{Green}}$	$\sqrt{\text{NIR} \times \text{Green}}$	

4.2. Creating a land cover map

ArcGIS 10.5 software was used to analyze satellite images captured in winter and summer when the total cloud cover was less than fifty percent. First, using the quality assessment ArcGIS tool and Landsat QA Pixel band, the cloud cover filter was applied, and low-quality pixels were disregarded. Using the instrument for cell statistics, the median seasonal image for each year was subsequently obtained. Finally, the maximum likelihood classification tool was used to classify seasonal images to determine the Al-Gharraf River's water body.

The classification of Landsat images required sample locations. Each year in the study area, a total of 2,000 random points from two categories, water and non-water, were selected at random. These points were labeled visually, and 75% of them were chosen at random for training, while the remaining 25% were chosen to validate the classifier. The spatial distribution of train and test sites is depicted in Figs. 4 and 5. With classification training, seasonal maps of water bodies in the study area were created. The median of these images was considered as the estimated boundary of the Al-Gharraf River (Fig. 6).

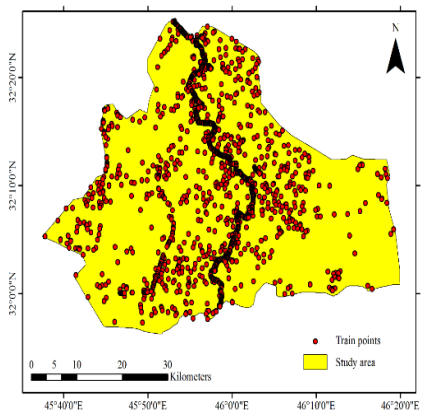

Fig. 4. Distribution map of train points

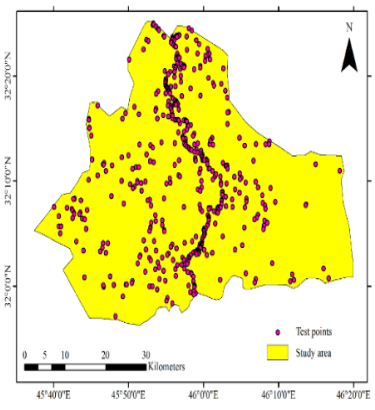

Fig. 5. Distribution map of test points

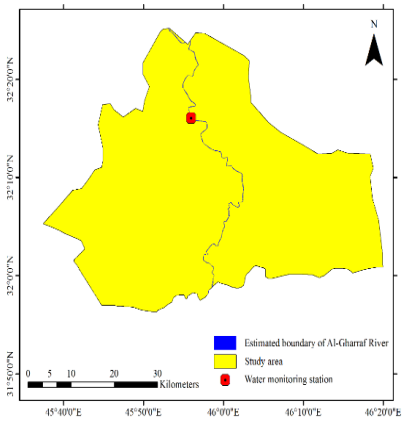

Fig. 6. Estimated boundary of Al-Gharraf River

4.3. Classification validation

Validation of land cover classification was performed using the confusion matrix and accuracy and precision criteria. Accordingly, 500 test points dispersed across the study area were used. On average, the MLC accuracy of train data and accuracy of test data were 0.954 and 0.936, respectively. Correspondingly, 0.970 and 0.957 were similar precision values. Classification validation results are summarized in Table 4.

Table 4. Validation of MLC model in land cover classification

Mean accuracy		**Mean precision**	
Train data	Test data	Train data	Test data
0.954	0.936	0.970	0.957

4.4. Monitoring changes in water dissolved substances

Using the Pearson coefficient, the correlation between water dissolved substances and spectral bands or indices of Landsat 8 images were calculated. Table 5 shows the correlation results. If we consider a value of 0-0.2 as very low correlation, value of 0.2-0.4 as low correlation, value of 0.4-0.6 as moderate correlation, value of 0.6-0.8 as high correlation, and value of 0.8-1 as very high correlation, according to Table 5, PO4 had only direct high correlation with NDWI (0.73) and a moderate inverse correlation with NDVI (-0.48), and it was not correlated with other spectral bands and indices. NO3 had very high direct correlations with SWIR 2 (0.94), SWIR 1 (0.93), SWIR 1 × Green (0.85), SWIR 2 × Green (0.85), NDVI (0.85), $\sqrt{\text{SWIR 1} \times \text{Green}}$ (0.84), $\sqrt{\text{SWIR 2} \times \text{Green}}$ (0.84), and NIR (0.85), respectively. Ca wasn't correlated with NDVI (0.01), had a high inverse correlation with NDWI (-0.7), SWIR 2 (-0.76), and SWIR 1 (-0.77), and had a very high inverse correlation with other spectral bands and indices. Mg had very high inverse correlation with NDVI (-0.89), SWIR 1 (-0.88), and SWIR 2 (-0.87), respectively. K had a moderate direct correlation with NDVI (0.61), wasn't correlated with NDWI (0.14), and had very high direct correlation with other spectral bands and indices. Na had the highest direct correlation with Blue (0.88), Red × Blue × Green (0.87), Red × Blue (0.87), $\sqrt{\text{Red} \times \text{Blue}}$ (0.86), $\sqrt{\text{Red} \times \text{Blue} \times \text{Green}}$ (0.86), Red (0.84), $\sqrt{\text{Red} \times \text{Green}}$ (0.84), Green (0.84), NIR × Green (0.80), and NDWI (0.80), respectively. SO4 wasn't correlated with NDWI (0.17) and had the highest inverse correlation with SWIR 1 (-0.93), SWIR 2 (-0.93), SWIR 1 × Green (-0.86), SWIR 2 × Green (-0.85), $\sqrt{\text{SWIR 1} \times \text{Green}}$ (-0.85), $\sqrt{\text{SWIR 2} \times \text{Green}}$ (-0.84), NDVI (-0.84), and NIR (-0.83), respectively. Cl had the highest direct correlation with Blue (0.66), NIR × Green (0.65), NIR (0.65), $\sqrt{\text{NIR} \times \text{Green}}$ (0.63), Red × Blue × Green (0.62), and SWIR 1 × Green (0.61), respectively. The highest inverse correlation for TDS was with NDWI (-0.79), Blue (-0.72), Red × Blue × Green (-0.70), and Red × Blue (-0.70), respectively. EC wasn't correlated with NDVI (0.12), had a moderate inverse correlation with SWIR 2 (-0.59), and had very high or high correlation with other spectral bands and indices. Finally, no significant correlation was observed for turb.

Table 5. Calculation of correlation between water quality parameters and spectral bands and indices of Landsat images

Parameters\Spectral band indices	**PO4**	**No3**	**Ca**	**Mg**	**K**	**Na**	**So4**	**Cl**	**TDS**	**EC**	**Turb**
Blue	0.22	0.62	-0.98	-0.58	0.88	0.88	-0.67	0.66	-0.72	-0.92	-0.12
Green	0.14	0.63	-0.98	-0.57	0.88	0.84	-0.66	0.59	-0.66	-0.90	-0.21
Red	0.17	0.57	-1.00	-0.49	0.84	0.84	-0.59	0.54	-0.66	-0.91	-0.25
NIR	0.01	0.81	-0.91	-0.76	0.97	0.76	-0.83	0.65	-0.57	-0.80	-0.15
SWIR 1	-0.21	0.93	-0.77	-0.88	1.00	0.57	-0.93	0.57	-0.37	-0.61	-0.19
SWIR 2	-0.24	0.94	-0.76	-0.87	0.99	0.55	-0.93	0.54	-0.34	-0.59	-0.22
NDVI	-0.48	0.85	0.01	-0.89	0.61	-0.08	-0.84	0.38	0.16	0.12	0.16
NDWI	0.73	-0.26	-0.70	0.26	0.14	0.80	0.17	0.34	-0.79	-0.82	0.02
Red × Green	0.17	0.59	-0.99	-0.53	0.85	0.85	-0.62	0.58	-0.68	-0.91	-0.21
Red × Blue	0.20	0.58	-0.99	-0.53	0.85	0.87	-0.62	0.60	-0.70	-0.92	-0.19
Red × Blue × Green	0.20	0.60	-0.99	-0.55	0.86	0.87	-0.64	0.62	-0.70	-0.92	-0.17
$\sqrt{\text{Red} \times \text{Green}}$	0.16	0.60	-0.99	-0.52	0.85	0.84	-0.62	0.56	-0.66	-0.90	-0.24
$\sqrt{\text{Red} \times \text{Blue}}$	0.18	0.59	-0.99	-0.53	0.85	0.86	-0.62	0.58	-0.68	-0.91	-0.21
$\sqrt{\text{Red} \times \text{Blue} \times \text{Green}}$	0.18	0.60	-0.99	-0.54	0.86	0.86	-0.63	0.59	-0.68	-0.91	-0.20
NIR × Green	0.07	0.75	-0.94	-0.71	0.95	0.80	-0.78	0.65	-0.62	-0.84	-0.15
SWIR 1 × Green	-0.07	0.85	-0.87	-0.80	0.99	0.70	-0.86	0.61	-0.50	-0.74	-0.19
SWIR 2 × Green	-0.08	0.85	-0.88	-0.79	0.98	0.69	-0.85	0.60	-0.49	-0.74	-0.21
$\sqrt{\text{NIR} \times \text{Green}}$	0.06	0.75	-0.94	-0.70	0.95	0.79	-0.77	0.63	-0.61	-0.84	-0.17
$\sqrt{\text{SWIR 1} \times \text{Green}}$	-0.08	0.84	-0.88	-0.78	0.98	0.70	-0.85	0.60	-0.50	-0.75	-0.20
$\sqrt{\text{SWIR 2} \times \text{Green}}$	-0.08	0.84	-0.88	-0.77	0.98	0.69	-0.84	0.58	-0.49	-0.75	-0.22

Using the calculated correlation values and weighted summation (Eq. 31), spatio-temporal monitoring of water dissolved substances of Al-Gharraf River was performed and estimation maps were created by ArcGIS 10.5 software. Figs. 7 to 17 show the estimation maps of water quality parameters of the Al-Gharraf River.

$$\text{Estimated parameter for each pixel} = \frac{\sum_{i=1}^{20} \text{Corr}(X_i,P) \times P_{\text{Pixel}}}{20} \quad (31)$$

In Eq. 31, X_i is the spectral band or index, P is the water quality parameter, P_{Pixel} is the water quality parameter of each pixel, and $\text{Corr}(X_i, P)$ is the correlation between the spectral band.

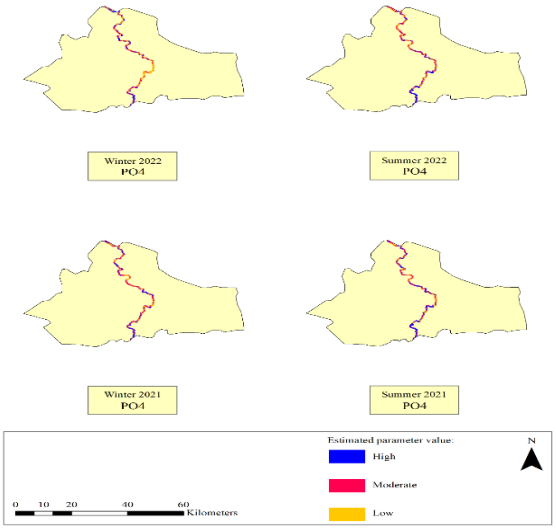

Fig. 7. Estimation map of PO4

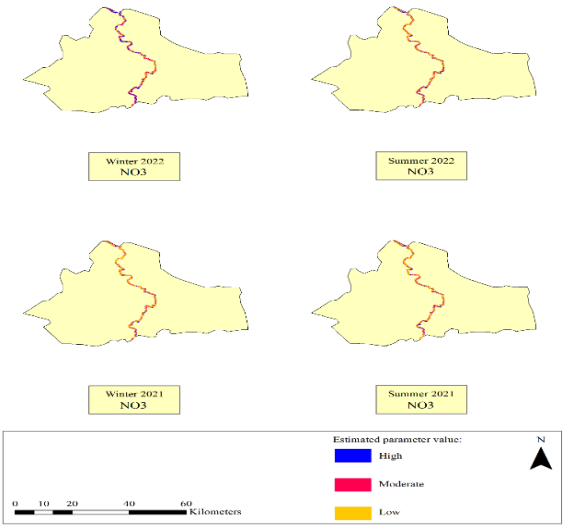

Fig. 8. Estimation map of NO3

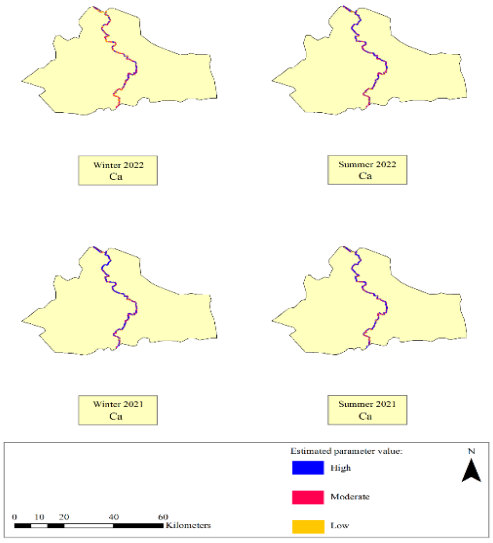

Fig. 9. Estimation map of Ca

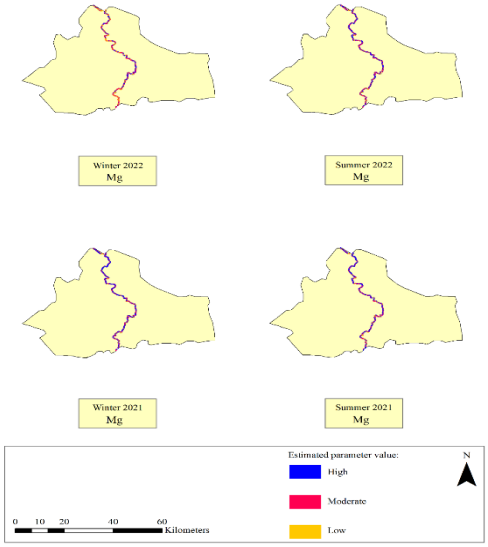

Fig. 10. Estimation map of Mg

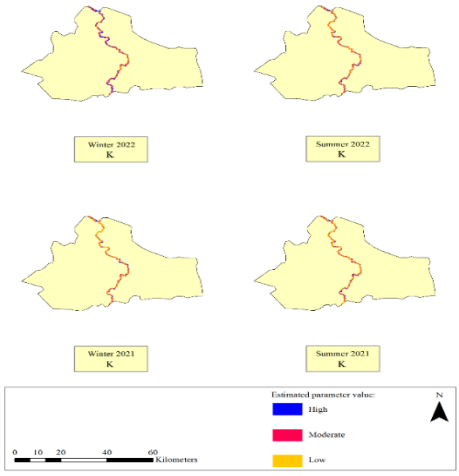

Fig. 11. Estimation map of K

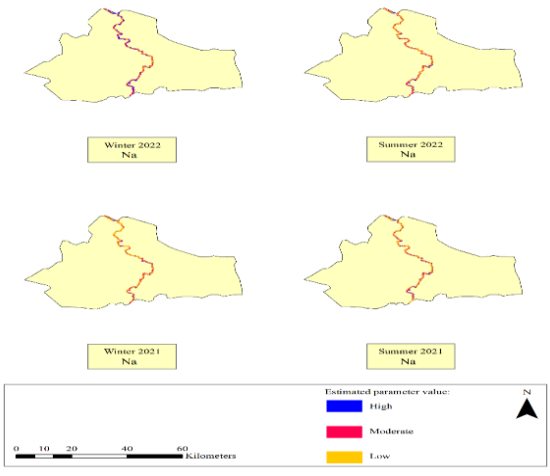

Fig. 12. Estimation map of Na

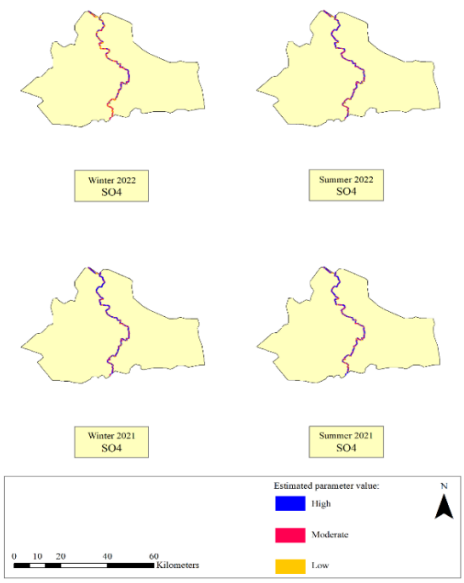

Fig. 13. Estimation map of SO4

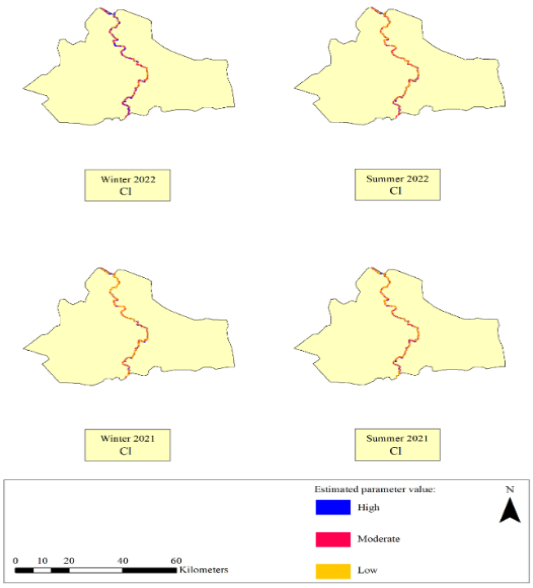

Fig. 14. Estimation map of Cl

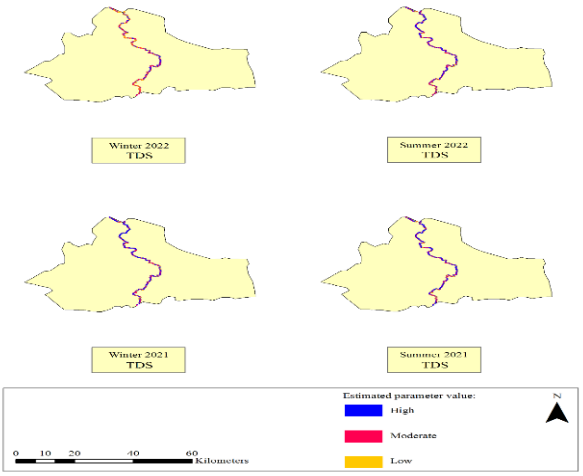

Fig. 15. Estimation map of TDS

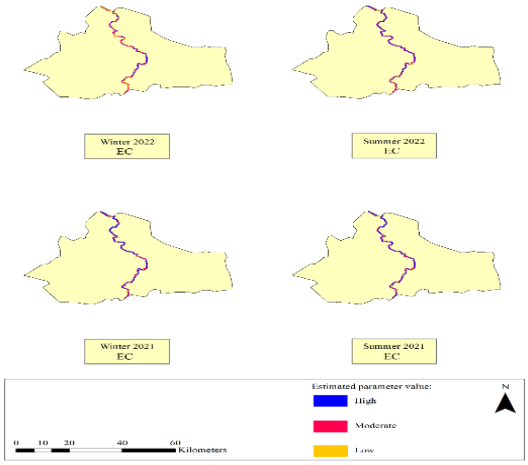

Fig. 16. Estimation map of EC

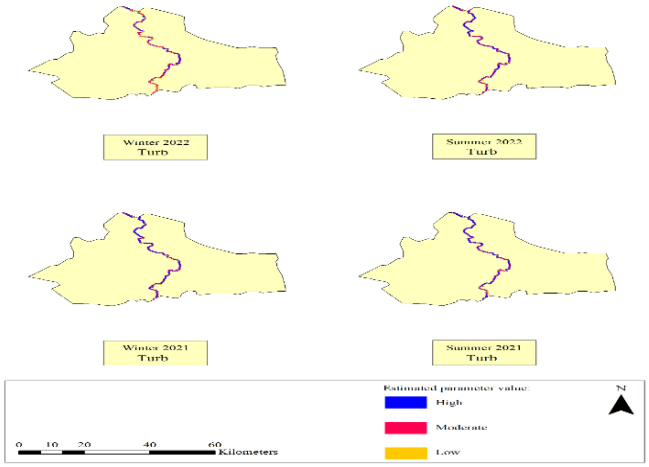

Fig. 17. Estimation map of Turb

The Mann-Kendall test was applied to understand the spatial trend, and graphing was used to determine the temporal trend of the Al-Gharraf River water quality parameters. Estimated parameters across the river were considered a data series for spatial trend analysis. Table 6 shows the results of spatial and temporal trend analysis. Table 6 Mann-Kendall test results for spatial trend analysis. D (Decreasing trend), I (Increasing trend).

Table 6. Mann-Kendall test results for spatial trend analysis (D (Decreasing trend), I (Increasing trend))

Parameter	Year	Season	Trend	P-Value	Z-Score	Mann-Kendall's score	Theil-Sen slope
Ca	2021	Winter	D	0	-15.97	-3461826	0
	2021	Summer	D	0	-23.38	-5072301	0
	2022	Winter	D	0.01	-2.52	-547209	0
	2022	Summer	D	0	-22.9	-4966527	0
CL	2021	Winter	I	0	15.87	3440974	0
	2021	Summer	I	0	22.34	4846105	0
	2022	Winter	I	0.01	2.74	593441	0
	2022	Summer	I	0	21.67	4700515	0
EC	2021	Winter	D	0	-15.98	-3465482	0
	2021	Summer	D	0	-23.8	-5161759	0
	2022	Winter	D	0.02	-2.4	5161759	0
	2022	Summer	D	0	-23.42	-5079165	0
K	2021	Winter	I	0	15.88	3444360	0
	2021	Summer	I	0	21.88	4745671	0
	2022	Winter	I	0	2.9	629037	0
	2022	Summer	I	0	21.09	4575365	0
Mg	2021	Winter	D	0	-15.78	-3421556	0
	2021	Summer	D	0	-20.49	-4445261	0
	2022	Winter	D	0	-3.25	-705317	0
	2022	Summer	D	0	-19.45	-4219415	0
Na	2021	Winter	I	0	15.97	3463756	0
	2021	Summer	I	0	23.77	5156459	0
	2022	Winter	I	0.0	2.4	520281	0
	2022	Summer	I	0	23.39	5073903	0
No3	2021	Winter	I	0	15.81	3428094	0
	2021	Summer	I	0	20.74	4499113	0
	2022	Winter	I	0	3.2	694227	0
	2022	Summer	I	0	19.72	4278257	0
Po4	2021	Winter	I	0	7.11	1541334	0
	2021	Summer	I	0	21.91	4753691	0
	2022	Winter	D	0	-3.18	-689647	0
	2022	Summer	I	0	29.03	6297133	0
So4	2021	Winter	D	0	-15.81	-3427706	0
	2021	Summer	D	0	-20.91	-4535137	0
	2022	Winter	D	0	-3.14	-681805	0
	2022	Summer	D	0	-19.93	-3467366	0
TDS	2021	Winter	D	0	15.99	-3467366	0
	2021	Summer	D	0	-24.31	-5273713	0
	2022	Winter	D	0.03	-2.24	-485983	0
	2022	Summer	D	0	-24.07	-5221917	0
Turb	2021	Winter	D	0	-16.13	-3498204	0
	2021	Summer	D	0	-23.56	-5109967	0
	2022	Winter	D	0.01	-2.68	-581789	0
	2022	Summer	D	0	-22.91	-4970169	0

By fitting 5th-degree polynomial functions, the temporal trend of the Al-Gharraf River water quality parameters from winter 2021 to summer 2022 was estimated. (Figs. 18 and 19) show the graphs of these functions.

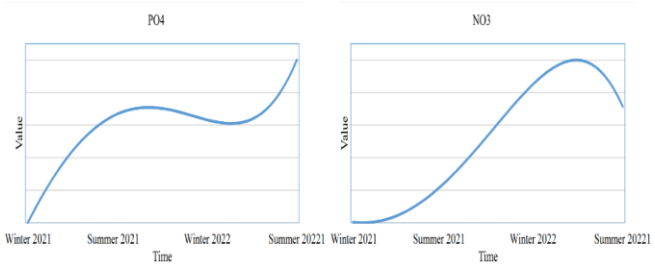

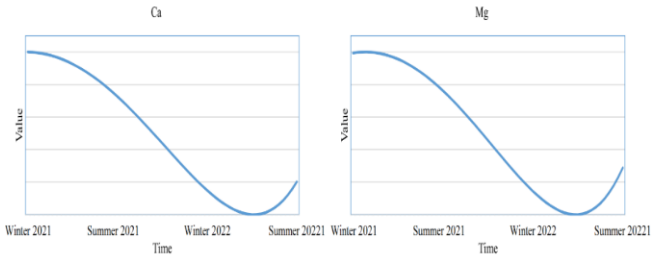

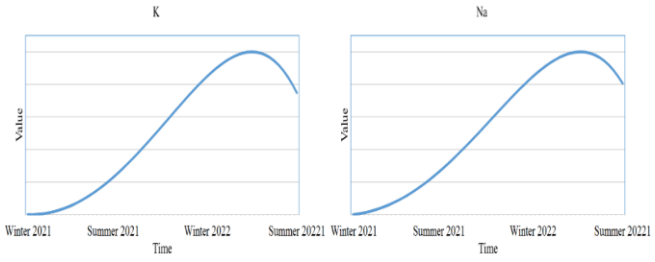

Fig. 18. Estimation of water quality parameters by 5th-degree polynomial

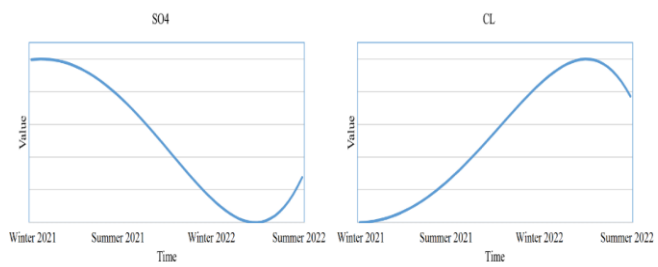

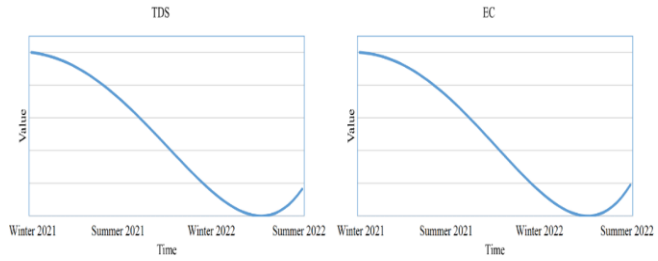

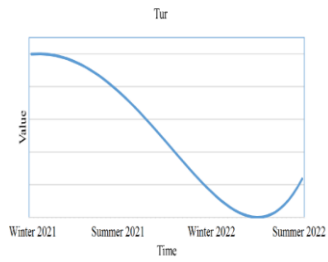

Fig. 19. Estimation of water quality parameters by 5th-degree polynomial

5. Discussion

In this research, multi-temporal maps of the change of dissolved substances in the waters of the Gharraf River were made by processing Landsat 8 images. In this regard, after processing the satellite images, the MLC classification was used to determine the water bodies in the region and the estimated limits of the Gharraf River were obtained. Although only one algorithm is used in this classifier, the high accuracy values of the MLC in both the training and test data indicate the excellent performance of this classifier. Then six spectral bands (blue, green, red, NIR, SWIR 1, and SWIR 2), two spectral indices, and 12 different combinations of spectral bands were calculated (Table 2). By establishing a remote sensing database, the correlation between water quality parameters and spectral bands and combinations of spectral bands was obtained. Consistent with previous studies [29], the observed correlation values showed that selected bands and band combinations are useful and provide useful information for water quality monitoring.

The results of temporal and spatial analysis showed the variation of dissolved substances in river water. The observed spatial changes had a uniform trend. The reason for this observation can be considered as the passage of the river through different land uses, the entry and exit of other waterways, and the entry of industrial, agricultural and urban wastewater. In each season, different values of solubility in river water were observed, but these changes did not have a clear direction. Precipitation and temperature are two factors that have a significant impact on water bodies. On the other hand, seasonal and annual changes in these two parameters were observed in Iraq [30]. Therefore, the effect of climatic factors on the water quality of Iraqi rivers is clear, and the reason for the seasonal changes of dissolved substances in the waters of the Gharraf River can be attributed to it. The main limitations of this research are the short period and the small number of field observations. In most studies, observations at a longer period and at different stations have been used [31]. However, the changes observed in the dissolved substances in the waters of the Gharraf River are remarkable. These changes can harm aquatic animal life, the environment, the health of citizens, and agricultural products. In general, it can be said that the use of spectral information from Landsat images is a practical method in the temporal and spatial monitoring of the quality and soluble matter in river water. This method can provide useful information to decision makers and officials.

6. Conclusion

This study was carried out to monitor the changes in dissolved substances in the water of the Al-Gharraf River using remote sensing. Based on this, the correlation between spectral bands, spectral indices, and different combinations of spectral bands of Landsat 8 images were measured with the observations of dissolved substances in river water at the water quality monitoring station, and the Mann-Kendall test evaluated the spatial trend of changes in dissolved substances in river water. The research results are as follows:

- The MLC algorithm had high precision and accuracy in classifying land cover and detecting water bodies. This algorithm is very popular in remote sensing classifications and is highly efficient.

- There was no significant difference between the average correlation between spectral bands, spectral indices, and combinations of spectral bands and water dissolved substances. As a result, the selected bands and band combinations are suitable for monitoring dissolved substances in river water.
- The spatial and temporal distribution of dissolved substances in Al-Gharraf river water is variable. Most of the spatial distributions had a uniform trend, while no specific trend was observed for the temporal distribution.
- The method presented in this research is practical and can be used for time-spatial analysis of the quality of water resources.

Acknowledgment

I would like to extend my sincere thanks and appreciation to those who helped me in this research; Dr. Ahmed Hussein Sultan, my colleague at the College of Engineering Technology, Baghdad, for the guidance they provided me during the preparation of this research.

References

[1] M. Gholizadeh, A. Melesse, L. Reddi, "A comprehensive review of water quality parameter estimation using remote sensing techniques," Journal in Sensors, Aug,2016, https://doi.org/10.3390/s16081298.
[2] E. T. Engman, R. J. Gurney, Chapman and Hall, "Remote sensing in hydrology," International Journal of Remote Sensing",0-412-24450-0. pp:1368, Nov,1991, https://doi.org/10.1080/01431169108955273
[3] A. Dekker, N. Zamurović, Ž., Hoogenboom, H., & Peters, S. "Remote sensing, ecological water quality modelling and in situ measurements: a case study in shallow lakes". Hydrological Sciences Journal,Vol.41,No.4,pp:.531-547,1996. https://doi.org/10.1080/02626669609491524
[4] W. Duan., He, B., Takara, K., Luo, P., Nover, D., Sahu, N., & Yamashiki, Y. (2013)." Spatio-temporal assessment of water quality incidents in Japan between 1996 and 2007". Journal in chemosphere, Vol.93, No 6, pp: 946-953, oct,2013 https://doi.org/10.1016/j.chemosphere.2013.05.060
[5] S. Ewad, "Concentration of some Heavy Elements in Water. Sediment and Plants in Al-Gharraf River in Thi-Qar Province –South of Iraq". Journal in University of Thi-Qar, 11, Dec, 2020. https://doi.org/10.32792/utq/utjsci/v7i2.716.
[6] S. Ewad, "Water quality assessment of the Gharraf River using two water quality indices" Applied Water Sciences". Iraqi Journal of Science, Vol. 57, No.2A, pp: 878-885,2016. https://doi.org/10.1007/s13201-016-0523-z
[7] M. Bonansea., A. Melesma, and L. Reddi." Using of new remote sensing satellites to assess reservoir water quality". Hydrological Sciences Journal, Vol. 64 No.1, pp:.34-44. published 2 Jan,2019 https://doi.org/10.1080/02626667.2018.1552001
[8] T. Lillesand, Kiefer, R. W., &J. Chipman, . "Remote Sensing and Image Interpretation". John Wiley & Sons. Journal Articel published 1 August 2015 in Photogrammetric Engineering. https://doi.org/10.14358/pers.81.8.615
[9] S. Ewad, and S. Abed. "Water Quality Index of Al-Gharraf River, Southern Iraq". Egyptian Journal of Aquatic Research, Vol.43 No2 ,pp: 117-122, published June 2017https://doi.org/10.1016/j.ejar.2017.03.001
[10] S. Pandey." Water pollution and Man's health". Kathmandu University medical journal (KUMJ), 4(1), pp:128-134, 2006, https://doi.org/10.5580/835.
[11] M Bonansea, A. Melesma, and L. Reddi. "Using new remote sensing satellites for assessing water quality in a reservoir". Hydrological Sciences Journal, 2, Janu, 2019. https://doi.org/10.1080/02626667.2018.1552001
[12] L. Olmanson, P. Brezonik , &M. Bauer. "Remote sensing for regional lake water quality assessment: capabilities and limitations of current and upcoming satellite systems". Book chapter, published in the Handbook of Environmental Chemistry. In Advances in watershed science and assessment (pp. 111-140), Springer,2015. https://doi.org/10.1007/978-3-319-14212-8_5.
[13] S. Ewaid, S. Abed. "Water quality index for Al-Gharraf river, southern Iraq". The Egyptian Journal of Aquatic Research, 43(2), No.117-122. published June 2017 https://doi.org/10.1016/j.ejar.2017.03.001.
[14] S. Taimi, Kalanga, H. Zvikomborero." Remote-sensing-based algorithms for water quality monitoring in olushanandja Dam, north -central Namibia". Issue:5, vol:21, pp:1878-1894, Aug,2021. https://doi.org/10.2166/ws.2020.290
[15] R D Jackson." Spectral indices in n-space". Journal Article published Nov, 1983, in Remote Sensing of Environment, 13(5), 409-421. https://doi.org/10.1016/0034-4257(83)90010-x.
[16] P. Macarof, F. Statescu," Comparison of NDBI and NDVI as indicators of surface urban heat island effect in Landsat 8 imagery :A case study of Iasi". PESD, VOL. 11, no. 2, 2017. DOI 10.1515/pesd-2017-0032
[17] N. Pettorelli. "The Normalized Difference Vegetation Index". Monograph published, 10, Oct, 2013, https://doi.org/10.1093/acprof:osobl/9780199693160.001.0001.
[18] B. C Gao." Normalized water difference index for remote sensing of plant liquid water from space. Remote Sensing of Environment". Journal Article published, Dec, 1996 in Remote Sensing of Environment https://doi.org/10.1016/s0034-4257(96)00067-3
[19] C. T Nguyen, A. Chidthaisong, P. K. Diem, & L.Huo, L. "A modified bare soil index to identify bare land features during agricultural fallow-period in southeast Asia using Landsat 8". Land, 10(3), 231. Journal Article, 25, Feb., 2021. in Land. https://doi.org/10.3390/land10030231.
[20] A. Malek, A. Chapok, M. Sultan, B. Hashim. H. Hussain and N. Al-Ansari. "Estimation of total dissolved solids in water bodies by spectral indicators: A case study". Journal Article September 2020 in Water, Air, & Soil Pollution https://doi.org/10.1007/s11270-020-04844-z.
[21] A. Ahmad, & S. Quegan, S." Analysis of Maximum Likelihood Classification Technique on Landsat 5 TM Satellite Data of Tropical Land Covers". November 2012 in 2012 IEEE International Conference on Control System, Computing and Engineering. https://doi.org/10.1109/iccsce.2012.6487156.
[22] T. Lillesand, R. W. Kiefer, & J. Chipman. "Remote Sensing and Image Interpretation". John Wiley & Sons. Journal Article published 1 August 2015 in Photogrammetric Engineering. https://doi.org/10.14358/pers.81.8.615.
[23] A. F. Militino, M. Ugarte, and U. Pérez-Gioia. "An introduction to the spatiotemporal analysis of satellite remote sensing data for geostatisticians". In Handbook of Mathematical Geosciences (pp. 239–253).2018. https://doi.org/10.1007/978-3-319-78999-6_13.
[24] S. Gog, and M. Dixit, M. "Conference on Advances in Signal Processing (CASP)", Publisher, IEEE, Jun, 2016; ISBN, 1509008497,

9781509008490. https://doi.org/10.1109/casp38054.2016.

[25] L. Hwang, and Ni, L. “Object-oriented classification of high-resolution satellite images for improved accuracy”. Spatial Resolution Assessment in Natural Resources and Environmental Sciences, IEEE, June 25-27, 2008. https://doi.org/10.1109/igarss.2008.4779519

[26] R.Goldblatt, , Yu, W, J .Hanson ., and A.K. Khandwal . “Detecting urban boundaries in India: A dataset for pixel-based image classification in Google Earth Engine”. Journal Article, 1, Aug, 2016. in Remote Sensing Remote Sensing, 8(8), 634. https://doi.org/10.3390/rs8080634

[27] M. Ansari, J. Nouri, and S. Fotohi, “Investigation of Temperature Precipitation and Flow Trend Using Nonparametric Man Kendall (Case Study: Kaju River in Sistan and Baluchistan)”. Journal watershed management research February 7(14):158-152,2017. https://doi.org/10.29252/jwmr.7.14.158.

[28] R. Goldblatt, Yu, W., J.Hanson, and A. Khandiwal. “Detecting urban boundaries in India: A dataset for pixel-based image classification in Google Earth Engine”. Journal Article 1 August 2016 in Remote Sensing Remote Sensing, 8(8), 634. https://doi.org/10.3390/rs8080634

[29] A. Maleki, A. Chapok., M.A.Sultan, B.M Hashim, H. M. Hussain, and N. Al-Ansari. “Estimation of total dissolved solids in water bodies by spectral indices case study: shatt al-Arab River”. Journal September 2020 in Water, Air, & Soil Pollution. https://doi.org/10.1007/s11270-020-04844-z.

[30] S. A.Salman, S. Shahid, T. Ismail, K. Ahmed, E. S. Chung, and X. J.Wang. “Characteristics of annual and seasonal trends of precipitation and temperature in Iraq”. Asia-Pacific Journal of Atmospheric Sciences, Aug, 55, 429-438, 2019. https://doi.org/10.1007/s13143-018-0073-4.

[31] W. Duan, K. Takara, He, B., Lu, P, D. Nofer, and Y. Yamashiki, “Spatial and temporal trends in estimates of nutrient and suspended sediment loads in the Ishikari River, Japan, from 1985 to 2010”, Journal in Science of the Total Environment, sept, 2013. https://doi.org/10.1016/j.scitotenv.2013.05.022.